

Active galactic nuclei in four metal-poor dwarf emission-line galaxies

Yuri I. Izotov

Main Astronomical Observatory, Ukrainian National Academy of Sciences, 27 Zabolotnoho str., Kyiv 03680, Ukraine

izotov@mao.kiev.ua

and

Trinh X. Thuan

Astronomy Department, University of Virginia, P.O. Box 400325, Charlottesville, VA 22904-4325

txt@virginia.edu

ABSTRACT

We present 3.5m Apache Point Observatory¹ second-epoch spectra of four low-metallicity emission-line dwarf galaxies discovered serendipitously in the Data Release 5 of the Sloan Digital Sky Survey (SDSS) to have extraordinary large broad H α luminosities, ranging from 3×10^{41} to 2×10^{42} erg s⁻¹. The oxygen abundance in these galaxies is very low, varying in the range $12 + \log \text{O}/\text{H} = 7.36 - 7.99$. Such extraordinarily high broad H α luminosities cannot be accounted for by massive stars at different stages of their evolution. By comparing with the first-epoch SDSS spectra, we find that the broad H α luminosities have remained constant over a period of 3 – 7 years, which probably excludes type II_n supernovae as a possible mechanism of broad emission. The emission most likely comes from accretion disks around intermediate-mass black holes with lower mass limits in the range $\sim 5 \times 10^5 M_{\odot} - 3 \times 10^6 M_{\odot}$. If so, these four objects form a new class of very low-metallicity AGN that have been elusive until now. The absence of the strong high-ionization lines [Ne v] $\lambda 3426$ and He II $\lambda 4686$ can be understood if the nonthermal radiation contributes less than $\sim 10\%$ of the total ionizing radiation.

¹The Apache Point Observatory 3.5-meter telescope is owned and operated by the Astrophysical Research Consortium.

Subject headings: galaxies: abundances — galaxies: irregular — galaxies: active
 – galaxies: ISM — H II regions — ISM: kinematics and dynamics

1. INTRODUCTION

Active galactic nuclei (AGN) are thought to be powered by massive black holes at the centers of galaxies, accreting gas from their surroundings. Observations of AGN show that they generally possess a high metallicity, varying from solar to supersolar metallicities (Storchi-Bergmann et al. 1998; Hamann et al. 2002). While the derived metallicities do depend on the detailed model assumptions, this appears to be a solid conclusion. Gas metallicity is known to be strongly correlated with the stellar mass of the host galaxy (Tremonti et al. 2004). Since AGN are usually found in massive, bulge-dominated galaxies that have converted most of their gas into stars by the present epoch, their gas metallicities are generally high. A question then arises: do low-metallicity AGN exist? If so, can we find them in low-mass galaxies? To address these questions, Groves et al. (2006) have searched the Sloan Digital Sky Survey (SDSS) Data Release 4 (DR4) spectroscopic galaxy sample of over 500,000 objects to select out $\sim 170,000$ emission-line galaxies with high S/N spectra. They then use diagnostic line ratios to select out 23,000 Seyfert 2s galaxies. Imposing an upper mass limit of $10^{10} M_{\odot}$ to restrict themselves to low-mass galaxies, they are left with a sample of only ~ 40 AGN, which they found appear to have metallicities around half that of typical AGN, i.e. having solar or slightly subsolar values. The same high metallicity range is found in the sample of low-mass AGN of Greene & Ho (2007b). Assessing their findings, Groves et al. (2006) are led to another question: “Why are there no AGN with even lower metallicities?” In this paper, we suggest that these low-metallicity AGN do exist although they are extremely rare.

In the course of a long-range program to search for extremely metal-deficient emission-line dwarf galaxies, Izotov et al. (2007b) have used the SDSS DR5 database of 675,000 spectra to assemble a large sample of emission-line galaxies. Two criteria were applied: 1) the [O III] $\lambda 4363$ line must be detected to allow for a direct determination of element abundances; and 2) obvious high-metallicity AGN spectra are excluded. Thus, contrary to Groves et al. (2006) and Greene & Ho (2007b), Izotov et al. (2007b) were not specifically looking for AGN. These criteria resulted in a sample of $\sim 10,000$ emission-line galaxies (ELG). While studying that sample to look for ELGs with broad components in their strong emission lines, Izotov et al. (2007b) came across four galaxies with very unusual spectra. The general characteristics of the four galaxies are given in Table 1. Their absolute magnitudes are typical of dwarf galaxies. Because of their relatively large distance ($z \sim 0.1-0.3$) and relatively small

angular sizes ($\sim 1''$ - $2''$, only slightly larger than the seeing disk), their SDSS images (Fig. 1) do not show much details. They possess a compact structure. Two galaxies, J1025+1402 and J1047+0739, have an approximately round shape, while the other two more distant galaxies, J0045+1339 and J1222+3602, have a distorted shape suggestive of mergers. Their colors are not blue like the other ELGs, but vary from red to yellow to green. Their spectra shown in Fig. 2, resemble those of moderately to very low-metallicity high-excitation H II regions: their oxygen abundances are in the range $12+\log \text{O}/\text{H} \sim 7.4$ – 7.9 , i.e. their heavy element mass fractions vary from $Z_{\odot}/19$ to $Z_{\odot}/5$ if the solar calibration $12+\log \text{O}/\text{H}=8.65$ of Asplund et al. (2005) is adopted. Izotov et al. (2007b) found that there is however a striking difference: the strong permitted emission lines, mainly the $\text{H}\alpha$ $\lambda 6863$ line, show very prominent broad components. These are characterized by somewhat unusual properties: 1) their $\text{H}\alpha$ full widths at zero intensity $FWZI$ vary from 102 to 158 Å, corresponding to expansion velocities between 2200 and 3500 km s^{-1} ; 2) the broad $\text{H}\alpha$ luminosities L_{br} are extraordinarily large, varying from 3×10^{41} to 2×10^{42} erg s^{-1} . This is to be compared with the range 10^{37} – 10^{40} erg s^{-1} found by Izotov et al. (2007b) for the other ELGs with broad-line emission. The ratio of $\text{H}\alpha$ flux in the broad component to that in the narrow component varies from 0.4 to 3.4, as compared to 0.01–0.4 for the other galaxies; 3) the Balmer lines show a very steep decrement, suggesting collisional excitation and that the broad emission comes from very dense gas ($N_e \gg 10^4 \text{ cm}^{-3}$). Evidently, these galaxies are exceedingly rare, since they constitute only 4/675,000 or 0.0006% of our original sample.

To account for the broad line emission in these four objects, Izotov et al. (2007b) have considered various physical mechanisms: a) Wolf-Rayet (WR) stars; b) stellar winds from Ofp or luminous blue variable stars; c) single or multiple Supernova (SN) remnants propagating in the interstellar medium; d) SN bubbles; e) shocks propagating in the circumstellar envelopes of type IIIn SNe; and f) AGN. While mechanisms a-d can account for $L_{br} \sim 10^{36}$ to 10^{40} erg s^{-1} , they cannot provide for luminosities that are 30 to 200 times greater. These very large luminosities are more likely associated with SN shocks or AGN. Izotov et al. (2007b) have considered type IIIn SNe because their $\text{H}\alpha$ luminosities are larger ($\sim 10^{38}$ – 10^{41} erg s^{-1}) than those of the other SN types, IIp and III, and they decrease less rapidly.

To decide whether type IIIn SNe or AGN are responsible for the broad emission in these galaxies, monitoring of their spectral features on the relatively long time scale of several years is necessary. If broad features are produced by IIIn type SNe, then we would expect a decrease in the broad line luminosities. No significant temporal evolution would be expected in the case of an AGN. Additionally, higher signal-to-noise ratio spectra are necessary to put better constraints on the presence of the high-ionization $[\text{Ne v}] \lambda 3426$ and $\text{He II} \lambda 4686$ emission lines, good indicators of a source of hard non-thermal radiation. In order to check for temporal evolution, we have obtained second-epoch spectra of the above four galaxies with

broad emission, using the 3.5m Apache Point Observatory (APO) telescope². We describe the observations in §2. We discuss in §3 the main properties of the broad emission and show that they can be accounted for by low-metallicity intermediate-mass AGN. Our conclusions are summarized in §4.

2. OBSERVATIONS

New high signal-to-noise ratio optical spectra were obtained for the four galaxies listed in Table 1, using the 3.5 m APO telescope on the nights of 2007 November 15 and 2008 February 6. The observations were made with the Dual Imaging Spectrograph (DIS) in the both the blue and red wavelength ranges. A $1''.5 \times 360''$ slit was used. In the blue range, we use the B400 grating with a linear dispersion of $1.83 \text{ \AA}/\text{pix}$ and a central wavelength of 4400 \AA , while in the red range we use the R300 grating with a linear dispersion $2.31 \text{ \AA}/\text{pix}$ and a central wavelength of 7500 \AA . The above instrumental set-up gave a spatial scale along the slit of $0''.8 \text{ pixel}^{-1}$ on the night of 2007 November 15 and of $0''.4 \text{ pixel}^{-1}$ on the night of 2008 February 6 (the latter scale is smaller by a factor of 2 than the previous one because we did not perform pixel binning for the latter spectra), a spectral range $\sim 3600 - 9600 \text{ \AA}$ and a spectral resolution of 7 \AA (FWHM). The slit was oriented along the parallactic angle and the total exposure time was 45 minutes for each galaxy. The observations were broken up into 3 subexposures to allow for removal of cosmic rays. The Kitt Peak IRS spectroscopic standard stars Feige 110 (2007 November 15), Feige 34 and G191B2B (2008 February 6) were observed for flux calibration. Spectra of He-Ne-Ar comparison arcs were obtained at the beginning of each night for wavelength calibration.

The data reduction procedures are the same as described in Thuan & Izotov (2005). The two-dimensional spectra were bias subtracted and flat-field corrected using IRAF. We then use the IRAF software routines IDENTIFY, REIDENTIFY, FITCOORD, TRANSFORM to perform wavelength calibration and correct for distortion and tilt for each frame. Night

²In fact, Izotov et al. (2007b) have identified 5 objects as AGN candidates. We have not included here the fifth candidate, J2230–0006≡PHL 293B, because its broad H α luminosity is only $8.6 \times 10^{37} \text{ erg s}^{-1}$, some $10^3 - 10^4$ times lower than those of the other four AGN candidates. The broad H α luminosity of J2230–0006 has been erroneously given in Table 8 of Izotov et al. (2007b) as having 10 times its true value. Given this relatively low luminosity and the fact that a new 3.5m APO spectrum of J2230–0006 shows that its broad hydrogen lines have a P Cygni profile with a blue-shifted absorption, the broad emission probably originates from a stellar wind rather than from an accretion disk around a AGN. Most likely, the broad emission in J2230–0006 is caused by a strong outburst in a bright luminous blue variable (LBV) star. Similar broad hydrogen emission has been detected recently by Pustilnik et al. (2008) in the extremely metal-deficient dwarf galaxy DDO 68.

sky subtraction was performed using the routine BACKGROUND. The level of night sky emission was determined from the closest regions to the galaxy that are free of galaxian stellar and nebular line emission, as well as of emission from foreground and background sources. A one-dimensional spectrum was then extracted from the two-dimensional frame using the APALL routine. An extraction aperture of $1''.5 \times 4''$ was adopted. Its area is similar to that of the $3''$ round aperture used in the SDSS spectra and allows to gather $\gtrsim 90\%$ of the light of our compact galaxies. Comparison of the line intensities of the SDSS (Izotov et al. 2007b) and 3.5m spectra (Table 2) shows that they agree well, validating our choice of the extraction aperture. Before extraction, the three distinct two-dimensional spectra of each object were carefully aligned using the spatial locations of the brightest part in each spectrum, so that spectra were extracted at the same positions in all subexposures. We then summed the individual spectra from each subexposure after manual removal of the cosmic rays hits.

The resulting APO spectra of the four galaxies are shown in Fig. 2. A strong broad $H\alpha$ emission line is present in all spectra, very similar to the one seen in the SDSS spectra of the same galaxies obtained 3–7 years earlier (Izotov et al. 2007b). The broad components in the $H\beta$ emission line are considerably weaker, suggesting a steep Balmer decrement and hence that the broad emission originates in a very dense gas. In the case of J1047+0739, broad He I is also present, as in the SDSS spectrum (Izotov et al. 2007b).

3. RESULTS AND DISCUSSION

3.1. Element abundances

We have derived element abundances from the narrow emission line fluxes. These fluxes have been measured using Gaussian fitting with the IRAF SPLOT routine. They have been corrected for both extinction, using the reddening curve of (Whitford 1958), and underlying hydrogen stellar absorption, derived simultaneously by an iterative procedure as described by Izotov et al. (1994) and using the observed decrements of the narrow hydrogen Balmer $H\delta$ $\lambda 4101$, $H\gamma$ $\lambda 4340$, $H\beta$ $\lambda 4861$ and $H\alpha$ $\lambda 6563$ lines. It is assumed in this procedure that hydrogen line emission is produced only by spontaneous transitions in recombination cascades, i.e. we neglect possible collisional excitation. Such a situation usually holds in low-density H II regions ionized by stellar radiation such as those considered here. Izotov et al. (2007a) have shown that the use of different reddening curves has little influence on the extinction-corrected fluxes (relative to the $H\beta$ flux) in the optical range and modify only slightly the extinction coefficient. The reason is that the spectra are corrected in such a way so that the relative intensities of the extinction-corrected hydrogen lines correspond

to their theoretical values. The extinction-corrected fluxes $100 \times I(\lambda)/I(\text{H}\beta)$ of the narrow lines for each galaxy, together with the extinction coefficient $C(\text{H}\beta)$, the equivalent width of the $\text{H}\beta$ emission line $\text{EW}(\text{H}\beta)$, the $\text{H}\beta$ observed flux $F(\text{H}\beta)$ and the equivalent widths of the underlying hydrogen absorption lines $\text{EW}(\text{abs})$ are given in Table 2. The physical conditions and element abundances of the H II regions in the four AGN candidates are derived from the narrow line fluxes following Izotov et al. (2006). The element abundances derived from the 2.5m SDSS spectra (Izotov et al. 2007b) and from the 3.5 m spectra (this paper) are shown in Table 3. We find the abundances and the abundance ratios obtained for the four galaxies from the two sets of observations agree well. The derived abundances are in the range characteristic of low-metallicity dwarf emission-line galaxies (Izotov et al. 2006). This implies that the narrow emission lines arise primarily from regions ionized by stellar ionizing radiation, and that any contribution of a possible AGN component to the narrow line emission is small.

3.2. Broad emission and diagnostic diagrams

Using Gaussian fitting, we have measured the fluxes of the broad component of the $\text{H}\alpha$ line after subtraction of the narrow component. These fluxes are shown in Table 4. Comparison of SDSS and APO broad $\text{H}\alpha$ fluxes shows that they have remained nearly constant (with variations $\leq 20\%$) over a period of $\sim 3 - 7$ years. This likely rules out the hypothesis that the broad line fluxes are due to type IIn SN because their $\text{H}\alpha$ fluxes should have decreased significantly over this time interval. There is one known exception, SN 1996cr, where the $\text{H}\alpha$ flux has remained constant for 7 yrs (Bauer et al. 2008), although here the luminosity of $\text{H}\alpha$ is only $\sim 10^{38}$ erg s $^{-1}$. Maintaining an $\text{H}\alpha$ luminosity of $10^{41} - 10^{42}$ erg s $^{-1}$ for such durations in our objects would require nearly the entire energy budget of a SN ($> 10^{50} - 10^{51}$ ergs). We thus rule out type IIn SNe.

There remains the AGN scenario. Can accretion disks around black holes in these low-metallicity dwarf galaxies account for their spectral properties? The spectra of the four objects do not show clear evidence for the presence of an intense source of hard nonthermal radiation: the [Ne v] $\lambda 3426$, [O II] $\lambda 3727$, He II $\lambda 4686$, [O I] $\lambda 6300$, [N II] $\lambda 6583$, and [S II] $\lambda \lambda 6717, 6731$ emission lines, which are usually found in the spectra of AGN, are weak or not detected. Aside from He II $\lambda 4686$, the apparent weakness of such emission lines, however, may be accounted for by the low metallicities of our galaxies. None of our objects were detected in the NVSS or FIRST radio catalogs, demonstrating that they are faint radio sources. Another way to check for the presence of an AGN in a galaxy is to check for its location in the emission-line diagnostic diagram of Baldwin et al. (1981) (BPT). It can be

seen that all four objects lie in the region corresponding to star-forming galaxies (SFG), to the left of the region occupied by AGN with low-mass black holes and with metallicities ranging from 2 to 1/4 that of the Sun (Greene & Ho 2007b). However, their locations in the SFG region do not necessarily disqualify them as AGN candidates. Photoionization models of AGN show that lowering their metallicity moves them to the left of the BPT diagram, so that they end up in the SFG region (Groves et al. 2006; Stasińska et al. 2006). Thus the BPT diagram is unable to distinguish between SFGs and low-metallicity AGN. Admitting that there is an AGN in our dwarf galaxies, can we account for the weakness of the high-ionization lines? Photoionization models with only AGN nonthermal ionizing radiation do predict detectable He II $\lambda 4686$ and [Ne V] $\lambda 3426$ emission lines. To make the observed spectra agree with the models, one solution is to dilute the nonthermal ionizing radiation from the AGN by thermal radiation from surrounding hot massive stars. In Fig. 3a, we show the results of our CLOUDY calculations (Ferland 1996; Ferland et al. 1998) of H II regions ionized by a composite radiation consisting of different proportions of stellar and nonthermal radiation. Two curves, characterized by different metallicities, are shown by solid lines: the lower one is for $12+\log O/H=7.3$ and the upper one is for $12+\log O/H=7.8$, typical of the metallicities of our objects. Each model point is labeled by the ratio R of nonthermal-to-thermal ionizing radiation. A slope $\alpha = -1$ has been adopted for the non-thermal power-law spectrum over the whole wavelength range under consideration ($f_\nu \propto \nu^\alpha$). The calculations have been done with a number of ionizing photons $Q_{th}=10^{53} \text{ s}^{-1}$ for stellar radiation, $Q_{nonth} = RQ_{th}$ for nonthermal radiation and $N_e=10^4 \text{ cm}^{-3}$. Higher densities would move the curves to the right. For the ionizing stellar radiation, we adopt Costar models by Schaerer & de Koter (1997) with a heavy element mass fraction $Z = 0.004$ and an effective temperature of 53,000K corresponding to a starburst age of $\lesssim 3 \text{ Myr}$. The dotted lines in Fig. 3a show the corresponding models with $\alpha = -2$. They are very similar to the models with $\alpha = -1$ when $R \leq 1$, but fall below for $R \gtrsim 1$. It is seen that models with $12+\log O/H=7.8$ and in which the nonthermal ionizing radiation contributes $\lesssim 10\%$ of the total ionizing radiation can account well for the location of all four galaxies in the BPT diagram, independently of the slope of the power-law spectrum.

How about the high-ionization lines? Can their absence be due to high dust extinction in the central part of the galaxy? We consider this possibility unlikely because in this case, broad H α emission from the accretion disk surrounding the black hole would not be seen also. We turn next to the properties of the ionizing spectrum for an explanation. In Fig. 3b, we show the diagnostic diagram for [Ne V] $\lambda 3426/H\beta$ vs. [N II] $\lambda 6583/H\alpha$ (thick lines) and He II $\lambda 4686/H\beta$ vs. [N II] $\lambda 6583/H\alpha$ (thin lines). As in Fig. 3a, CLOUDY models with $\alpha = -1$ and -2 are shown by solid and dotted lines. They are also characterized by $Q_{th}=10^{53} \text{ s}^{-1}$ for stellar radiation, $Q_{nonth} = RQ_{th}$ for nonthermal radiation and $N_e=10^4 \text{ cm}^{-3}$. Higher

densities would shift curves to the right. The vertical dashed line separates models with $12+\log\text{O}/\text{H} = 7.3$ (Fig. 3b, left) from those with $12+\log\text{O}/\text{H} = 7.8$ (Fig. 3b, right). The shaded rectangle shows the region of the upper limits of $\sim 1\%$ - 2% of the $\text{H}\beta$ flux, set for $[\text{Ne v}] \lambda 3426/\text{H}\beta$ and $\text{He II } \lambda 4686/\text{H}\beta$ in our objects, in the observed range of their $[\text{N II}] \lambda 6583/\text{H}\alpha$ ratio. There are several points to be made concerning Fig. 3b. First, in contrast to the low-ionization line fluxes (Fig. 3a), the predicted fluxes of the high-ionization lines are more strongly dependent on the slope of the power-law spectrum of the nonthermal radiation. Second, while there is no significant change of the predicted fluxes of the $\text{He II } \lambda 4686$ emission line with metallicity, the predicted flux of the $[\text{Ne v}] \lambda 3426$ linearly scales with $12+\log\text{O}/\text{H}$. Third, at a given metallicity, the detectability of the high-ionization lines depends on two parameters: one is the ratio R of nonthermal-to-thermal ionizing radiation and the other is the slope of the power-law ionizing spectrum. If we adopt $12+\log\text{O}/\text{H} = 7.8$ as typical for our galaxies, then Fig. 3b shows that models that satisfy the non-detectability limit of the high-ionization lines (i.e. that fall within the shaded box) are characterized either by a steep slope and a not excessively small R ($\alpha = -2$ and $R \sim 0.1$) or by a shallower slope and a very low R ($\alpha = -1$ and $R \sim 0.03$). We expect intermediate-mass black holes to have accretion disks that are hotter than those around supermassive black holes, and hence their ionizing spectrum to have a shallower slope, nearer -1 rather than -2 . If that is the case, then the fraction of ionizing nonthermal to thermal radiation is very small in our dwarf galaxies, $\sim 3\%$. It is also possible that the absence of strong high-ionization lines is caused by a high covering factor of the accretion disk. In this case the hard radiation would be absorbed inside the dense accretion disk and no high-ionization forbidden lines would be formed.

3.3. Black hole virial masses

We now estimate the masses of the central black holes. It has been shown (see e.g. Kaspi et al. 2000) that continuum and broad line luminosities in AGN can be used to determine the size and geometry of the broad emission-line region and the mass of the central black hole. Examining a large sample of broad-line AGN, Greene & Ho (2005) have found that the $\text{H}\alpha$ luminosity scales almost linearly with the optical continuum luminosity and that a strong correlation exists between the $\text{H}\alpha$ and $\text{H}\beta$ line widths. On the basis of these two empirical correlations, those authors have derived the following relations for the central black hole mass:

$$M_{\text{BH}} = 2.0 \times 10^6 \left(\frac{L_{\text{H}\alpha}}{10^{42} \text{ergs s}^{-1}} \right)^{0.55} \left(\frac{\text{FWHM}_{\text{H}\alpha}}{10^3 \text{km s}^{-1}} \right)^{2.06} M_{\odot}, \quad (1)$$

$$M_{\text{BH}} = 4.4 \times 10^6 \left(\frac{L_{5100}}{10^{44} \text{ergs s}^{-1}} \right)^{0.64} \left(\frac{\text{FWHM}_{\text{H}\beta}}{10^3 \text{km s}^{-1}} \right)^2 M_{\odot}, \quad (2)$$

where $L_{\text{H}\alpha}$ and L_{5100} are respectively the broad $\text{H}\alpha$ and continuum (at $\lambda = 5100\text{\AA}$) luminosities, and $\text{FWHM}_{\text{H}\beta}$ and $\text{FWHM}_{\text{H}\alpha}$ are respectively the full widths at half maximum of the $\text{H}\beta$ and $\text{H}\alpha$ emission lines.

In Table 5 we list the extinction-corrected broad $\text{H}\alpha$ luminosities $L(\text{H}\alpha)$ and continuum luminosities $\lambda L_{\lambda}(5100)$ for the four galaxies, as derived from the SDSS spectra. The extinction coefficient was set equal to the one derived for the narrow Balmer hydrogen lines. Since the reddening due to dust extinction in dense regions may be larger than that derived from the narrow hydrogen emission lines, the derived $L(\text{H}\alpha)$ should be considered as lower limits. The $L(\text{H}\alpha)$ and $\lambda L_{\lambda}(5100)$ of our galaxies follow closely the correlation between $\text{H}\alpha$ and continuum luminosities found by Greene & Ho (2005). This implies that our galaxies are very likely the same type of objects as those considered by Greene & Ho (2005). Therefore, we can use Eqs. 1 – 2 for the determination of the central black hole masses. For the flux and luminosity determinations, we first fit the line profiles by a single Gaussian. However, we find that single Gaussian fits do not reproduce well the broad low-intensity wings of the $\text{H}\alpha$ line. This suggests that that the line broadening is caused not only by gas motions but also by light scattering. This hypothesis is supported by a steep Balmer decrement (the $\text{H}\alpha$ -to- $\text{H}\beta$ flux ratio is greater than ~ 7 in our four galaxies), implying high gas densities and possibly high optical depths in the $\text{H}\alpha$ line. Therefore, in addition to a single Gaussian profile fit, we have also fitted the $\text{H}\alpha$ line by a Voigt profile which is a superposition of both a Gaussian profile and a Lorentzian profile. In Table 5, we show the FWHMs of the Gaussian components in both cases. The FWHMs are smaller by a factor of $\lesssim 2$ in the case of the Voigt profile fitting as compared to the single Gaussian fitting. For the central black hole mass determination, we have adopted the Gaussian FWHMs derived from the more accurate Voigt profile fitting. We have also set $\text{FWHM}_{\text{H}\beta}$ to be equal to $\text{FWHM}_{\text{H}\alpha}$, following Greene & Ho (2005). The masses $M_{\text{BH}}(\text{H}\alpha)$ and $M_{\text{BH}}(5100)$ derived from the broad $\text{H}\alpha$ and continuum luminosities are shown in Table 5. The masses derived from the two methods are in good agreement, as expected from the relation between $L(\text{H}\alpha)$ and $\lambda L_{\lambda}(5100)$ for our objects and the correlation between the $\text{H}\alpha$ and continuum luminosities found by Greene & Ho (2005). The derived masses of the central black holes in our galaxies are in the range $\sim 5 \times 10^5 M_{\odot} - 3 \times 10^6 M_{\odot}$, lower or similar to the mean black hole mass of $1.3 \times 10^6 M_{\odot}$ found by Greene & Ho (2007b) for their sample of low-mass black holes. Since the luminosities used to derive the masses of the central black holes are lower limits, the derived masses should also be considered as lower limits.

4. CONCLUSIONS

We study here the broad line emission in four low-metallicity star-forming dwarf galaxies with $12+\log\text{O}/\text{H} \sim 7.4 - 8.0$, i.e. with metallicities between 1/19 and 1/5 that of the Sun. We have arrived at the following conclusions:

1. The steep Balmer decrements of the broad hydrogen lines and the very high luminosities of the broad $\text{H}\alpha$ line in all four galaxies (3×10^{41} to 2×10^{42} erg s⁻¹) suggest that the broad emission arises from very dense and high luminosity regions such as those associated with supernovae (SNe) of type II_n or with accretion disks around black holes. However, the relative constancy of the broad $\text{H}\alpha$ luminosities over a period of 3–7 years likely rules out the SN mechanism. Thus, the emission of broad hydrogen lines is most likely associated with accretion disks around black holes. If so, these four objects would harbor a new class of AGN that are extremely rare (in 0.0006% of all galaxies). These AGN would be intermediate-mass black holes residing in low-metallicity dwarf galaxies, with an oxygen abundance that is considerably lower than the solar or super-solar metallicity of a typical AGN.

2. There is no obvious spectroscopic evidence for the presence of a source of a non-thermal hard ionizing radiation in all four galaxies: high-ionization emission lines such as He II $\lambda 4686$ and [Ne v] $\lambda 3426$ emission lines were not detected at the level $\leq 1 - 2$ percent of the $\text{H}\beta$ flux. We have calculated a series of CLOUDY models with ionizing spectra which include both thermal stellar and nonthermal power-law ionizing radiation in order to account for the absence of the high-ionization lines. We find that the predicted fluxes of the high-ionization lines are below the detectability level if the spectral energy distribution $f_\nu \propto \nu^\alpha$ of the ionizing nonthermal radiation has $\alpha \sim -1$ and the nonthermal ionizing radiation is significantly diluted by the thermal stellar ionizing radiation contributing $\lesssim 3$ percent of the total ionizing radiation, or the ionizing spectrum is steeper ($\alpha \sim -2$), and the nonthermal ionizing radiation contributes $\lesssim 10$ percent of the total ionizing radiation.

3. The lower limits of the masses of the central black holes M_{BH} of $\sim 5 \times 10^5 M_\odot - 3 \times 10^6 M_\odot$ in our galaxies are among the lowest found thus far for AGN.

George Privon, George Trammell and David Whelan kindly obtained the spectrum of J0045+1339 for us. We thank Franz Bauer and John Hawley for useful discussions. Luis Ho and the referee provided very helpful comments on the manuscript. Y.I.I. is grateful to the staff of the Astronomy Department at the University of Virginia for their warm hospitality. We thank the financial support of National Science Foundation grant AST02-05785. The 3.5 APO time was available thanks to a grant from the Frank Levinson Fund of the Silicon Valley Community Foundation to the Astronomy Department of the University of Virginia.

Funding for the Sloan Digital Sky Survey (SDSS) and SDSS-II has been provided by the Alfred P. Sloan Foundation, the Participating Institutions, the National Science Foundation, the U.S. Department of Energy, the National Aeronautics and Space Administration, the Japanese Monbukagakusho, the Max Planck Society, and the Higher Education Funding Council for England.

REFERENCES

- Asplund, M., Grevesse, N., & Sauval, A.J. 2005, ASP Conf Ser. 336: Cosmic Abundances as Records of Stellar Evolution and Nucleosynthesis, 336, 25
- Baldwin, J. A., Phillips, M. M., & Terlevich, R. 1981, PASP, 93, 5
- Bauer, F. E., Dwarkadas, V. V., Brandt, W. N., Immler, S., Smartt, S., Bartel, N., & Bietenholz, M. F. 2008, ApJ, in press; (arXiv:0804.3597)
- Ferland, G. J. 1996, Hazy: A brief Introduction to CLOUDY (Univ. Kentucky Dept. Phys. Astron. Internal Rep.)
- Ferland, G. J., Korista, K. T., Verner, D. A., Ferguson, J. W., Kingdon, J. B., & Verner, E. M. 1998, PASP, 110, 761
- Greene, J. E. & Ho, L. C. 2005, ApJ, 630, 122
- Greene, J. E. & Ho, L. C. 2007a, ApJ, 667, 131
- Greene, J. E. & Ho, L. C. 2007b, ApJ, 670, 92
- Groves, B. A., Heckman, T. M., & Kauffmann, G. 2006, MNRAS, 371, 1559
- Hamann, F. et al. 2002, ApJ, 564, 592
- Izotov, Y. I., Thuan, T. X., & Lipovetsky, V. A. 1994, ApJ, 435, 647
- Izotov, Y. I., Stasińska, G., Meynet, G., Guseva, N. G., & Thuan T. X. 2006, A&A, 448, 955
- Izotov, Y. I., Thuan, T. X., & Stasinska, G. 2007a, ApJ, 662, 15
- Izotov, Y. I., Thuan, T. X., & Guseva, N. G. 2007b, ApJ, 671, 1297
- Kauffmann, G., et al. 2003, MNRAS, 346, 1055
- Kaspi, S., Smith, P. S., Netzer, H., Maoz, D., Jannuzi, B. T., & Giveon, U. 2000, ApJ, 533, 631
- Pustilnik, S. A., Teplyakova, A. L., Kniazev, A. Y., & Burenkov, A. N. 2008, MNRAS, in press; preprint arXiv:0805.3551
- Schaerer, D., & de Koter, A. 1997, A&A, 322, 598
- Stasińska, G., Cid Fernandes, R., Mateus, A., Sodré, L., Jr., & Asari, N. V. 2006, MNRAS, 371, 972

Storchi-Bergmann, T., Smitt, H. R., Calzetti, D., & Kinney, A. L. 1998, *AJ*, 115, 909

Thuan, T. X., & Izotov, Y. I. 2005, *ApJS*, 161, 240

Tremonti, C. A., et al. 2004, *ApJ*, 613, 898

Whitford, A. E. 1958, *AJ*, 63, 201

Table 1. General characteristics of low-metallicity AGN candidates

Object	R.A. (J2000.0)	DEC. (J2000.0)	Redshift	g	M_g
SDSSJ0045+1339	00 45 29.2	+13 39 09	0.29522	21.80	−18.56
SDSSJ1025+1402	10 25 30.3	+14 02 07	0.10067	20.36	−17.66
SDSSJ1047+0739	10 47 55.9	+07 39 51	0.16828	19.91	−19.23
SDSSJ1222+3602	12 22 45.7	+36 02 18	0.30112	21.30	−19.10

Table 2. Intensities of narrow emission lines from 3.5m spectra

ION	$100 \times I(\lambda)/I(\text{H}\beta)$	$100 \times I(\lambda)/I(\text{H}\beta)$	$100 \times I(\lambda)/I(\text{H}\beta)$	$100 \times I(\lambda)/I(\text{H}\beta)$
	Galaxy			
	J0045+1339	J1025+1402	J1047+0739	J1222+3602
3727 [O II]	65.45 ± 2.47	70.06 ± 6.30	94.18 ± 2.20	41.36 ± 2.27
3868 [Ne III]	50.42 ± 2.05	56.01 ± 5.29	52.64 ± 1.35	64.17 ± 2.68
3889 He I + H8	...	20.40 ± 4.21	18.17 ± 1.02	12.74 ± 3.01
3968 [Ne III] + H7	29.75 ± 2.51	40.16 ± 4.88	33.31 ± 1.18	47.17 ± 3.50
4026 He I	1.18 ± 0.65
4101 H δ	25.04 ± 2.84	24.47 ± 4.42	26.78 ± 1.10	26.95 ± 2.80
4340 H γ	43.49 ± 2.49	50.40 ± 5.80	45.90 ± 1.30	44.38 ± 4.01
4363 [O III]	14.78 ± 1.59	24.44 ± 2.98	10.68 ± 0.50	20.77 ± 1.76
4471 He I	5.03 ± 0.33	...
4861 H β	100.00 ± 3.12	100.00 ± 13.09	100.00 ± 2.24	100.00 ± 6.33
4959 [O III]	244.61 ± 5.94	200.48 ± 14.85	183.36 ± 3.48	283.29 ± 7.73
5007 [O III]	747.92 ± 17.18	575.78 ± 34.53	555.65 ± 10.10	853.85 ± 22.21
5876 He I	20.38 ± 0.62	...
6563 H α	279.78 ± 13.73	271.10 ± 82.71	281.42 ± 9.24	277.54 ± 14.82
6583 [N II]	6.54 ± 1.03	4.06 ± 1.18	4.50 ± 0.09	...
6678 He I	6.15 ± 0.27	...
6717 [S II]	6.53 ± 0.26	...
6731 [S II]	4.23 ± 0.24	...
7065 He I	28.89 ± 0.74	...
7136 [Ar III]	5.00 ± 0.26	...
$C(\text{H}\beta)$	0.135	0.110	0.400	0.100
EW(H β) Å	394	45	116	196
$F(\text{H}\beta)^{\text{a}}$	0.12	0.16	0.70	0.14
EW(abs) Å	5.55	0.10	5.35	5.50

^ain units 10^{-14} erg s $^{-1}$ cm $^{-2}$.

Table 3. Element abundances

Object	2.5m SDSS			3.5m APO		
	$12+\log \text{O}/\text{H}$	$\log \text{N}/\text{O}$	$\log \text{Ne}/\text{O}$	$12+\log \text{O}/\text{H}$	$\log \text{N}/\text{O}$	$\log \text{Ne}/\text{O}$
J0045+1339	7.94 ± 0.08	-1.23 ± 0.17	-0.77 ± 0.15	7.86 ± 0.05	-1.14 ± 0.08	-0.83 ± 0.07
J1025+1402	7.36 ± 0.08	-1.16 ± 0.30	-0.86 ± 0.14	7.48 ± 0.08	-1.30 ± 0.14	-0.74 ± 0.12
J1047+0739	7.99 ± 0.05	-1.21 ± 0.09	-0.73 ± 0.09	7.85 ± 0.02	-1.46 ± 0.03	-0.68 ± 0.04
J1222+3602	7.94 ± 0.09	-1.02 ± 0.24	-0.84 ± 0.14	7.88 ± 0.05	...	-0.70 ± 0.07

Table 4. Fluxes of the broad H α emission line at different epochs

Object	2.5m SDSS			3.5m APO	
	I_{br} ^a	I_{br}/I_{nar} ^b	Date of Obs.	I_{br} ^b	Date of Obs.
J0045+1339	16.4 \pm 1.7	41.65	2000 Jan 12	18.0 \pm 0.7	2007 Nov 15
J1025+1402	165.0 \pm 5.7	337.49	2004 Mar 11	192.5 \pm 0.8	2008 Feb 06
J1047+0739	289.2 \pm 9.1	122.34	2003 Jan 31	224.2 \pm 2.1	2008 Feb 06
J1222+3602	16.1 \pm 1.8	71.69	2005 Mar 13	22.4 \pm 1.3	2008 Feb 06

^aIn units 10^{-16} erg s $^{-1}$ cm $^{-2}$. Flux errors are derived taking into account photon statistics in non-flux calibrated spectra.

^bIn percent.

Table 5. $H\alpha$ and continuum luminosities and masses of the black holes^a

Object	$L_{br}(H\alpha)^b$	FWHM $_{br}(H\alpha)$		$\lambda L_\lambda(5100)^b$	$M_{BH}(H\alpha)^f$	$M_{BH}(5100)^f$
		Gaussian ^{c,d}	Voigt ^{c,e}			
J0045+1339	2.74×10^{41}	1700	1540	7.59×10^{42}	2.43×10^6	2.00×10^6
J1025+1402	3.21×10^{41}	1580	680	3.62×10^{42}	5.07×10^5	2.50×10^5
J1047+0739	1.57×10^{42}	1920	1050	2.32×10^{43}	3.05×10^6	1.91×10^6
J1222+3602	2.80×10^{41}	1600	790	7.17×10^{42}	6.34×10^5	5.10×10^5

^aParameters are derived from the 2.5 m SDSS spectra (Izotov et al. 2007b).

^bIn units erg s^{-1} .

^cIn units km s^{-1} .

^dDerived by fitting a Gaussian profile.

^eDerived by fitting a Voigt profile, a combination of Gaussian and Lorentzian profiles. The FWHM is that of the Gaussian profile.

^fIn solar masses.

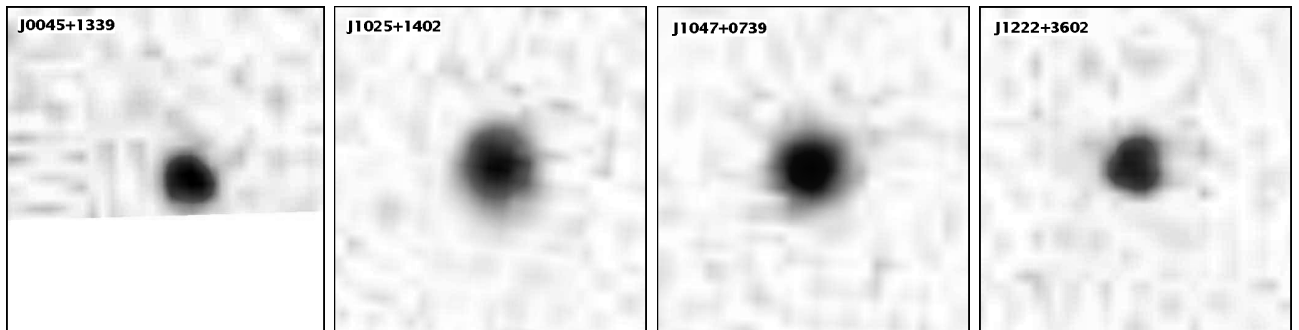


Fig. 1.— $13'' \times 13''$ SDSS images of low-metallicity AGN. The angular diameters of the objects vary between $1''$ and $2''$, barely larger than the seeing disk.

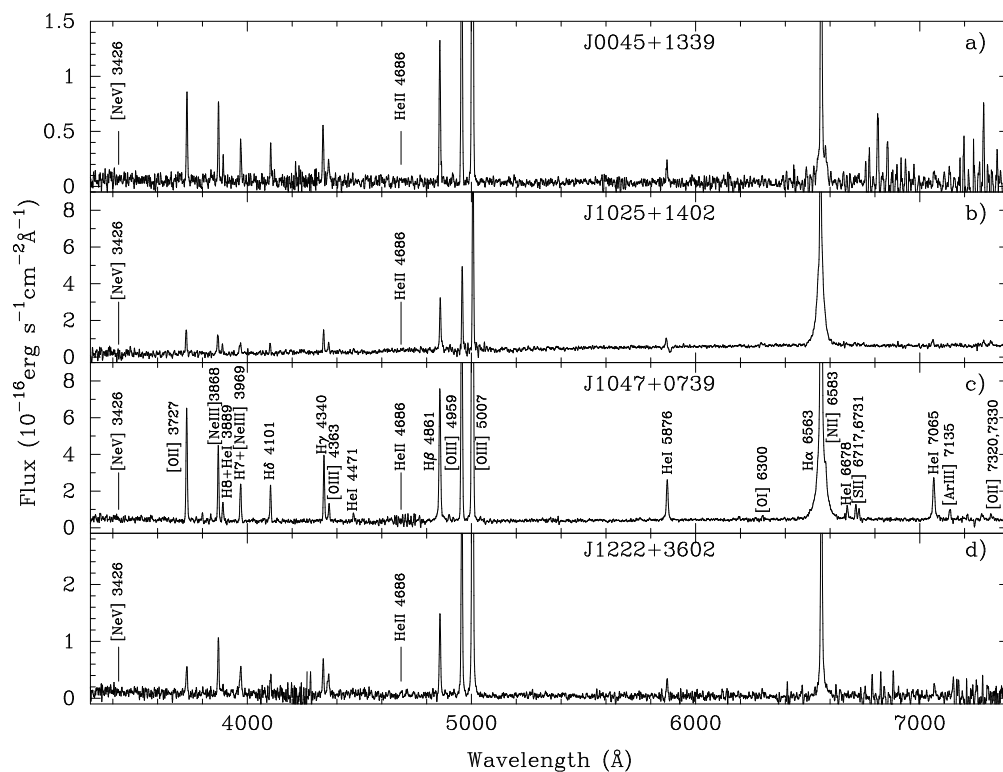


Fig. 2.— Redshift-corrected 3.5 m Apache Observatory second-epoch spectra of four low-metallicity emission-line dwarf galaxies thought to contain AGN. The locations of the non-detected [Ne v] $\lambda 3426$ and He II $\lambda 4686$ high-ionization emission lines are shown in all panels. Other emission lines are labeled in panel c).

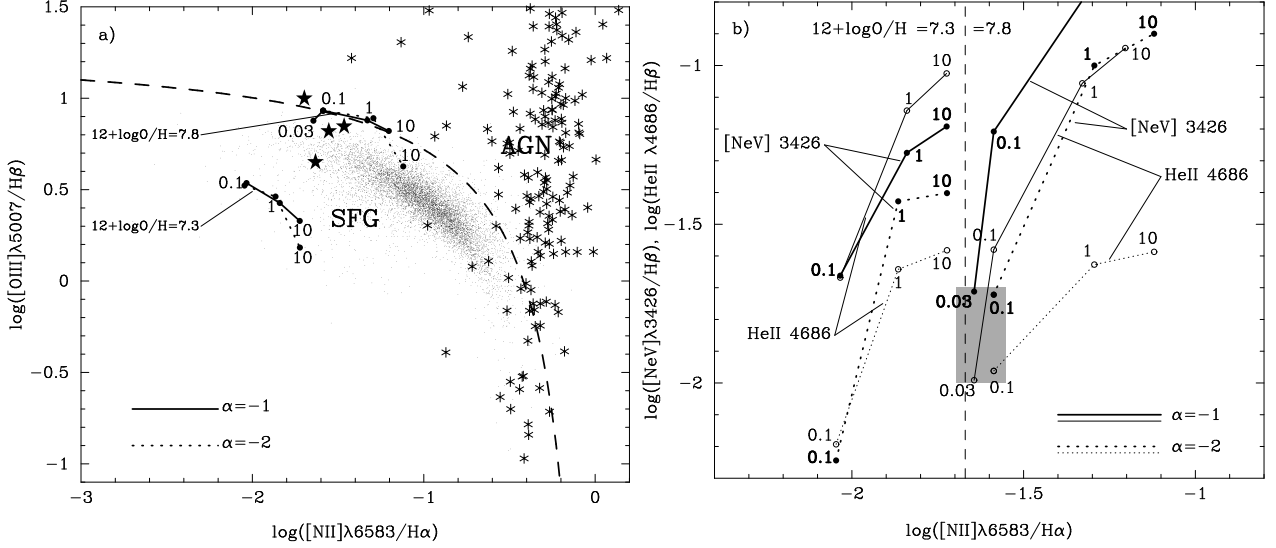


Fig. 3.— a) The BPT diagram (Baldwin et al. 1981) for low-ionization emission lines. Plotted are the $\sim 10,000$ ELGs from Izotov et al. (2007b) (cloud of points), the low-mass black hole sample of Greene & Ho (2007b) (asterisks) and the four low-metallicity AGN in Table 1 (stars). The dashed line separates star-forming galaxies (SFG) from active galactic nuclei (AGN) (Kauffmann et al. 2003). The solid and dotted lines connect CLOUDY photoionization models computed for H II regions ionized by a composite radiation consisting of different proportions of stellar and nonthermal radiation. The two upper curves are characterized by $12+\log \text{O}/\text{H} = 7.8$ and the two lower ones by $12+\log \text{O}/\text{H} = 7.3$. Each model point is labeled by the ratio of nonthermal-to-thermal ionizing radiation. All curves have been calculated adopting a number of ionizing photons $Q = 10^{53} \text{ s}^{-1}$ for stellar radiation, different slopes of the nonthermal spectral energy distributions $f_\nu \propto \nu^\alpha$ (solid lines are for $\alpha = -1$ and dotted lines are for $\alpha = -2$). A density $N_e = 10^4 \text{ cm}^{-3}$ is adopted. Higher densities would shift the curves to the right. b) The diagnostic diagram for high-ionization emission lines: $[\text{Ne V}]\lambda 3426/\text{H}\beta$ vs. $[\text{N II}]\lambda 6583/\text{H}\alpha$ (thick lines) and $\text{He II}\lambda 4686/\text{H}\beta$ vs. $[\text{N II}]\lambda 6583/\text{H}\alpha$ (thin lines). The same CLOUDY models as in a) are shown. The shaded region shows the upper intensity limits of the high-ionization lines $[\text{Ne V}]\lambda 3426$ and $\text{He II}\lambda 4686$ relative to $\text{H}\beta$ in the four galaxies considered here. The dashed vertical line separates models with $12+\log \text{O}/\text{H} = 7.30$ (left) from those with $12+\log \text{O}/\text{H} = 7.80$ (right).